ACS APPLIED MATERIALS & INTERFACES

Letter

www.acsami.org

Robust Thin-Film Generator Based on Segmented Contact-Electrification for Harvesting Wind Energy

Xian Song Meng,[†] Guang Zhu,*[,†,‡] and Zhong Lin Wang*[,†,‡]

[†]Beijing Institute of Nanoenergy and Nanosystems, Chinese Academy of Sciences, Beijing 100083, China

[‡]School of Material Science and Engineering, Georgia Institute of Technology, Atlanta, Georgia 30332, United States

Supporting Information

ABSTRACT: Collecting and converting energy from ambient air flow promise to be a viable approach in developing self-powered autonomous electronics. Here, we report an effective and robust triboelectric generator that consists of an undulating thin-film membrane and an array of segmented fine-sized electrode pairs on a single substrate. Sequential processes of contact electrification and electrostatic induction generate alternating flows of free electrons when the membrane interacts with ambient air flow. Based on an optimum rational design, the segmented electrodes play an essential role in boosting the output current, leading to an enhancement of over 500% compared to the structure without the segmentation. The thin-film based generator can simultaneously and continuously light up tens of commercial light-emitting diodes. Moreover, it possesses exceptional durability, providing constant electric output after millions of operation cycles. This work offers a truly practical solution that opens the avenue to take advantage of wind energy by using the triboelectric effect.

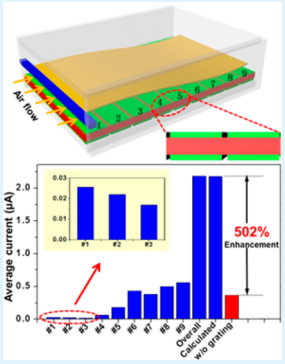

KEYWORDS: *energy harvesting, wind energy, triboelectric effect, self-powered electronics*

1. INTRODUCTION

Harvesting energy from nature is an important route in obtaining clean and sustainable energy.[1,2] Wind, as one of the most common renewable energy sources, is being increasingly utilized as a result of worldwide efforts.[3−7] In general, energy conversion for this purpose is realized through generators that rely on electromagnetic effect.[8−11] Recently, triboelectric generators (TEG) based on the coupling of triboelectric effect and electrostatic induction have been developed as a new means of harvesting mechanical energy;[12−16] and they have been demonstrated in collecting wind energy.[17,18] In comparison to traditional electromagnetic generators, the TEG-based wind harvester featured high power density, light weight, simple structure, and low cost,[19−21] making it especially suitable as a power source for autonomous electronics. In a previous work,[18] a plastic thin film fluttered as driven by air flow, resulting in reciprocating contact with another material that had different triboelectric polarity in order to generate a periodically changing electric field for alternating current (ac) output. However, it was found in this work that asynchronous oscillation of the membrane led to serious "inner consumption" due to counteracting effect from different sections of the membrane, which largely deteriorated the output power of the TEG. Besides, electrodes that were fabricated on the regularly strained thin film had a high risk of fatigue failure, which posed a problem in robustness for practical applications.

Herein, we first report a new design of triboelectric generator for harvesting wind energy, in which all electrodes are integrated onto a single stationary substrate. Because the electrodes are no longer subject to periodic strain, the newly designed TEG owns exceptional stability and does not have any measurable decay in the output current after continuous operation for millions of cycles. Then, we further introduce segmentation of electrodes by using an array of fine electrode pairs; and each pair serves as an individual unit. Compared with the design without the electrode array, the segmented triboelectric generator (S-TEG) properly solves the problem of "inner consumption", leading to a gigantic enhancement by more than 500% in average current. It is successfully demonstrated as a power source for simultaneously and continuously lighting up tens of commercial light-emitting diode (LED) bulbs. Therefore, this work presents a key step toward practical use of contact electrification in harvesting wind energy.

2. EXPERIMENTAL SECTION

Fabrication of the TEG. An acrylic sheet was cut into dimensions of 9 cm × 5 cm × 3 mm through laser cutting. On both sides of the sheet, aluminum electrodes (200 nm in thickness) were deposited by e-beam evaporation. A polyimide thin film (Kapton) of 30 μm in thickness was used as the undulating membrane. It was fixed to an acrylic supporting beam that had a separation of 0.5 cm away from the underlying electrode. A through case fabricated by acrylic sheets was used to enclose the entire structure and to create a confined channel for conducting air flow. The height of the channel was 1.5 cm.

Received: March 24, 2014
Accepted: May 13, 2014
Published: May 13, 2014

   dx.doi.org/10.1021/am501782f | ACS Appl. Mater. Interfaces 2014, 6, 8011−8016

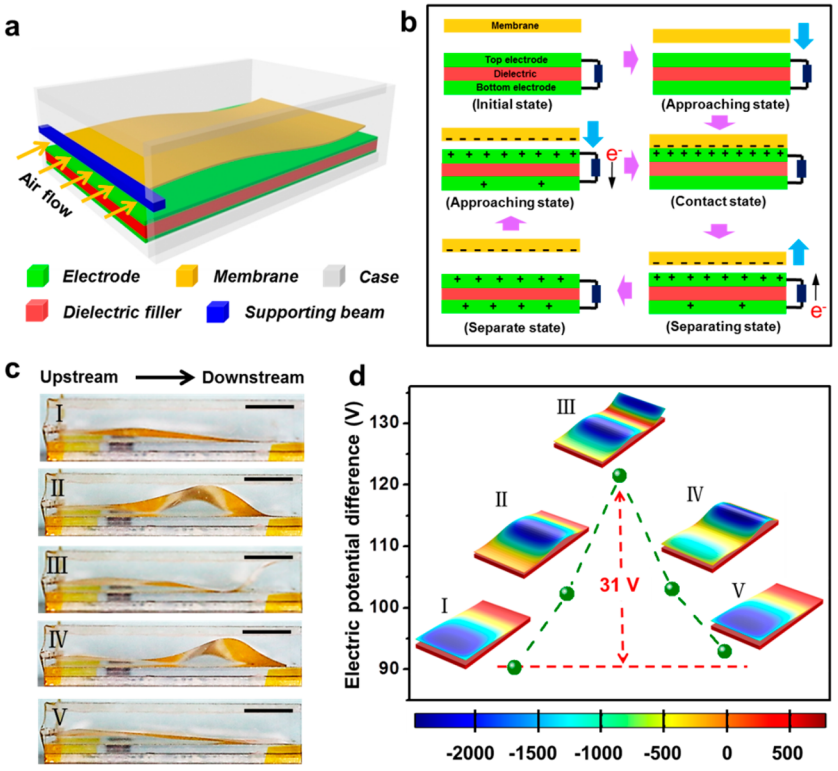

Figure 1. Structural design and operating principle of a triboelectric generator. (a) Schematic diagram of the triboelectric generator without segmentation. (b) Illustration of the basic electricity-generating process based on a simplified model in which the membrane keeps flat when moving up and down. (c) Actual profiles of the oscillating membrane captured in photographs at five different typical states, clearly showing the undulating behavior of the membrane. (d) Electric potential difference between the two electrodes at the five states shown in (c). Insets with rainbow coloring are simulation results via COMSOL that show the electric potential distribution.

Two copper wires were connected to the electrodes for electric measurement. The fabrication process of a segmented TEG is similar but with an additional step. After electrodes were deposited on the acrylic substrate, both sides were cut by laser to create shallow trenches that defined the segments. There are nine segmented electrodes on each side, with every segment having a lateral dimension of 5 cm × 1 cm.

Theoretical Simulation via COMSOL. 3D models were built, which matched actual profiles of the undulating membrane at certain states. In open-circuit condition, the bottom surface of the membrane was assigned a surface charge density of -8×10^{-6} C/m[24] and the top electrode was assigned a total surface charge of 3.6×10^{-8} C. In short-circuit condition, the membrane surface was assigned a surface charge density of -8×10^{-6} C/m^2, whereas the two electrodes were set as a terminal with a fixed charge quantity of 3.6×10^{-8} C.

3. RESULTS AND DISCUSSION

The structure of the TEG without segmented electrodes is shown in Figure 1a. Two electrodes are spaced out by a dielectric filling layer in between. The upstream side of a flexible membrane is fixed to a supporting beam that has a separation away from the electrode underneath in the vertical direction, while the downstream side is left free-standing. A through acrylic case is then used to enclose the entire structure, which creates a confined channel for conducting air flow (see Figure S1 in the Supporting Information). Two lead wires are connected to the electrodes for electric measurement.

For discussion on the basic principle of energy generation, the membrane is simplified into a flat surface that vertically moves, as shown in Figure 1b. Once the membrane is in physical contact with the top electrode, electrons are transferred from the metal electrode to the membrane surface due to contact electrification governed by different triboelectric polarities of materials.[22] This process produces negative and positive triboelectric charges that can stay on the membrane and on the top electrode, respectively.[23] As the membrane is separating away from the top electrode (Figure 1b), free electrons flow through external loads from the bottom electrode to the top electrode in order to balance out the charge distribution between the two electrodes.[24] As the membrane approaches the top electrode again, the negative surface charges drive free electrons back to the bottom electrode. Therefore, reciprocating motion of the membrane generates alternating current between the two electrodes.

In actual situation, vertical movement of the membrane is realized when air flow is laterally directed into the TEG. Since the supporting beam has the shape of a bluff body, it regularly sheds alternating vortices on either side of the membrane when nonturbulent air flows in parallel to the device.[25−27] The resulting pressure differential caused by the vortices forces the flexible membrane to move in an oscillating motion,[28−30] thus bringing the membrane into repeated contact with the electrode that is placed beneath. In Figure 1c, profiles of the membrane at five typical undulating states are captured and numbered from state I to state V. In open-circuit condition, corresponding electric potential difference across the electrodes ($U_{top}-U_{bottom}$) at each state is obtained through finite element simulation via COMSOL and then plotted in Figure 1d. It can be found that the electric potential difference varies in a

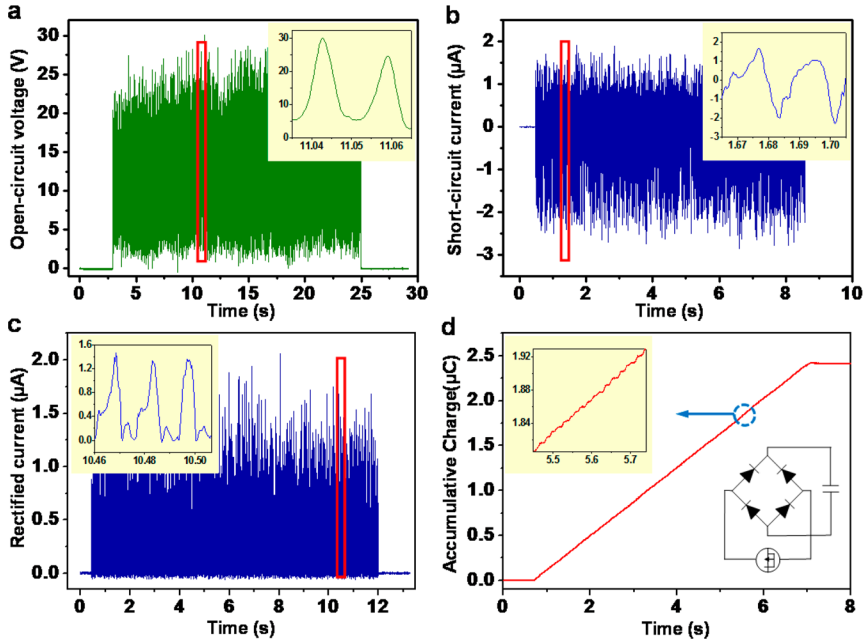

Figure 2. Electric measurement results of a triboelectric generator without segmentation. (a) Open-circuit voltage; inset: enlarged view enclosed by the red frame. (b) Short-circuit current; inset, enlarged view enclosed by the red frame. (c) Rectified current without extra load; inset, enlarged view enclosed by the red frame. (d) Accumulative charge from the rectified current in c; inset, enlarged view enclosed by the blue circle (left) and circuit diagram of the measurement (right). All measurement results were obtained at a flow rate of 12.6 m/s.

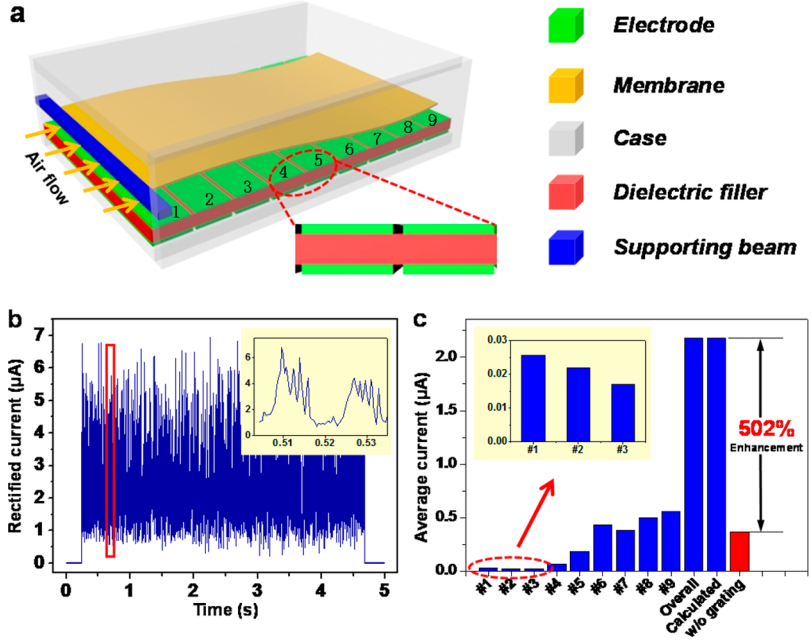

Figure 3. Triboelectric generator that has segmented electrodes. (a) Schematic diagram of the triboelectric generator with segmented electrodes; inset: enlarged cross-sectional view showing the arrangement of electrodes on both sides. (b) Rectified current without extra load; inset: enlarged view enclosed by the red frame. (c) Average current from each unit numbered from 1 to 9; the measured overall average current equals with the calculated summation of currents from all single units and presents an enhancement by 502% compared to the generator without segmentation (red column). All measurement results were obtained at a flow rate of 12.6 m/s.

repeated way. It is the variance of the electric potential distribution that serves as the driving force for electron flows. Detailed simulation settings are presented in the Experimental Section; and zoom-in views of all simulated plots are shown in Figure S2 in the Supporting Information.

To experimentally obtain output characteristics of the TEG, we used compressed air through a pressure regulator to generate air flow with adjustable rate. Open-circuit voltage (V_{oc}) and short-circuit current (I_{sc}) measured at a flow rate of 12.6 m/s are presented in Figure 2a and 2b, respectively. The V_{oc} oscillates between zero and a peak value of 30 V at a frequency of 103 Hz (inset of Figure 2a). The measured peak-to-peak value of V_{oc} agrees well with the simulated value in Figure 1d. The I_{sc} exhibits an ac behavior, which is also

dx.doi.org/10.1021/am501782f | ACS Appl. Mater. Interfaces 2014, 6, 8011−8016

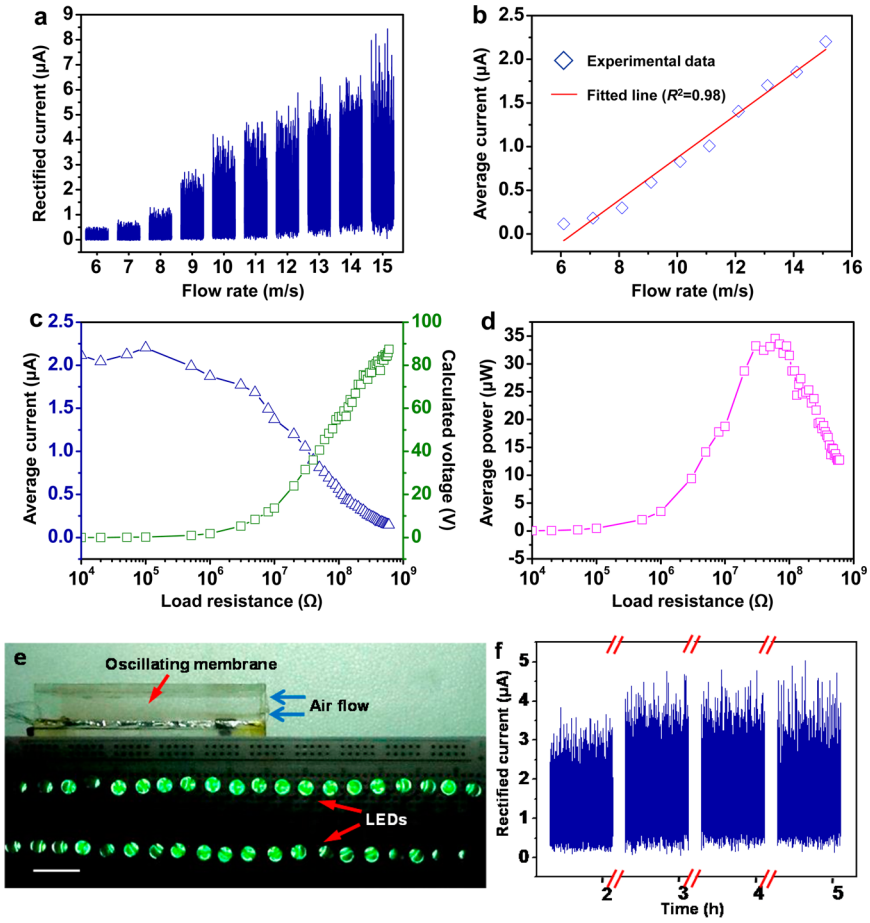

Figure 4. Output characteristics of a triboelectric generator with segmented electrodes. (a) Rectified current without extra load and (b) average current as a function of varying flow rates. (c) Dependence of the average current, calculated voltage, and (d) calculated average output power on the load resistance. The load matching test was conducted at a flow rate of 12 m/s. (e) Photograph of the triboelectric generator as a power source for simultaneously lighting up 40 LED bulbs. (f) Durability test on rectified current for ~2 million cycles in 5 h at a flow rate of 12 m/s.

consistent with the theoretical analysis above. However, it is observed that the negative current peaks are larger than the positive ones in amplitude (Figure 2b). This difference is likely attributed to asymmetric movement of the membrane when it is approaching or separating from the top electrode. Additional weight of the membrane and the electrostatic attraction from the charged top electrode are likely reasons that result in the faster approaching process. Consequently, current peaks that correspond to this process have larger amplitude. The ac output can be transferred to pulsed direct current simply through a full-wave rectifying bridge (Figure 2c). The rectified current provides an unidirectional charge flow that can buildup constructively. As illustrated in Figure 2d, the accumulative charges reach 2.4 μC in 6.3 s, corresponding to an average direct current of 0.38 μA.

However, as discussed above, the actual movement of the membrane deviates from the simplified illustration in Figure 1b. When the membrane flutters, every point on the membrane along the direction of air flow vertically oscillates but has phase difference compared to adjacent points, similar to the case of traveling waves. As a consequence, different sections of the membrane exert partially counteracting effects on the variation of electric potential, which results in largely diminished electric output. As a solution to this problem, a segmented-structured TEG (S-TEG) was developed. As shown in Figure 3a, both of the electrodes are segmented into a linear array of strip-shaped units with uniform width (see Figure S3 in the Supporting Information and the Experimental Section for the fabrication process). Here, a total of nine segments are formed and numbered in sequence from upstream to downstream in Figure 3a. Each fine segment has a pair of electrodes and can be considered as a reduced-sized TEG that operates independently. For each segment that has very limited span in the flow direction, the maximum phase difference within corresponding section of the membrane is substantially reduced. The electric output from each segment is first individually rectified and then added up in parallel with the same polarity. Figure 3b displays the I_{sc} of the S-TEG, which has apparently larger amplitude compared to one without segments in Figure 2c. Detailed examination on an enlarged view yields identification of a series of small current peaks in sequence within a large current peak (inset of Figure 3b). They are attributed to current output from adjacent segments, clearly indicating that the electric output from the segments are partially overlapped with apparent phase difference. To clearly prove the superiority of the segment structure, the average dc current from each segment is individually measured and presented in Figure 3c. The ones at the upstream produce much less current than those positioned at the downstream. This is because the membrane has much less undulating amplitude at the upstream and results in smaller change in separation distance away from the electrode. The measured overall average current by connecting

dx.doi.org/10.1021/am501782f | ACS Appl. Mater. Interfaces 2014, 6, 8011−8016

all segments in parallel exactly matches the calculated result obtained by summation of the measured current from each segment. In comparison to a nonsegmented TEG of the same size, the average current gigantically increases by over 500% (Figure 3c), explicitly demonstrating the effectiveness of the segmented design.

Furthermore, theoretical simulation yields a similar enhanced result (see the Supporting Information, Note 1 and Figure S4). It is also worth noting that the number of segments is an important factor for the enhancement. The simulation results in Figure S4d in the Supporting Information indicate that our fabricated device is rationally designed and optimized, which can achieve good performance with minimum structural complexity.

The electric output of the S-TEG has a strong correlation with the air flow rate. Panels a and b in Figure 4 show that the amplitude of the I_{sc} and the corresponding average current substantially increase with the flow rate, respectively. The good linearity (R^2 = 0.98) obtained in Figure 4b suggests a potential application of the S-TEG as a self-powered wind vector sensor. To further investigate the characteristics of the S-TEG as a power source, load matching test was systematically conducted, with the external load resistance ranging from 1 Ω to 600 MΩ. Figure 4c exhibits the dependence of the average dc current ($I_{average}$) and corresponding calculated voltage on the load resistance. It is found that the average current decreases with the load while the calculated voltage has a reverse trend, producing an optimum average output power ($I^2_{average}R$) of 35 μW at a matched load of 60 MΩ (Figure 4d). When directly connected to commercial light-emitting diode (LED) bulbs, the S-TEG simultaneously and continuously lighted up 40 of them (Figure 4e and Movie 1 in the Supporting Information), explicitly demonstrating the capability of the S-TEG in powering small electronics. Durability test at a flow rate of 12 m/s proves the stability and reliability of this design. The rectified current does not show any observable decay after continuous operation for 5 h, corresponding to approximately 2 million cycles of oscillation (Figure 4f). Furthermore, the dependence of the electric output on the air flow angle was also investigated in both horizontal dimension and vertical dimension. As shown in Figure S5 in the Supporting Information, the S-TEG can still produce 65% and 75% of the electric output even when the air flow is 20° off the axis in the horizontal and the vertical dimensions, respectively.

4. CONCLUSION

In summary, we made key progress toward practical use of triboelectric generators for harvesting wind energy by solving two major issues. First, segmentation of electrodes properly solves the problem of "inner consumption" resulting from the oscillating nature of the membrane, leading to tremendous improvement on the electric output. Second, all electrodes are fully imbedded and secured in the new design here, which ensures long-term stability and reliability of the generator. Because of the small size and light weight due to use of thin-film materials, the generator can be further scaled up not only in area but also in volume by stacking layers of units in the vertical dimension for more effectively making use of wind energy possibly on a large scale.

■ ASSOCIATED CONTENT

Supporting Information

Profile of a triboelectric generator without segmentation, simulation results that show the electric potential distributions for the five states defined in Figure 1c, simulation results of charge transfer in short-circuit condition for a nine-unit S-TEG. This material is available free of charge via the Internet at http://pubs.acs.org.

■ AUTHOR INFORMATION

Corresponding Authors

*E-mail: gzhu7@gatech.edu.
*E-mail: zhong.wang@mse.gatech.edu.

Notes

The authors declare no competing financial interest.

■ ACKNOWLEDGMENTS

The research was supported by the "thousands talents" program for pioneer researcher and his innovation team, China, Beijing City Committee of science and technology project (Z131100006013004). Patents have been filed based on the research presented here.

■ REFERENCES

(1) Williams, J. L.; Alhajji, A. The Coming Energy Crisis. *Oil Gas J.*. **2003**, *101*.
(2) El Baradei, M. A Global Agency Is Needed for the Energy Crisis. *Financ. Times* **2008**, *23*.
(3) Kaldellis, J. K.; Zafirakis, D. The Wind Energy (R) Evolution: A Short Review of a Long History. *Renewable Energy* **2011**, *36*, 1887−1901.
(4) Blanco, M. I. The Economics of Wind Energy. *Renewable Sustainable Energy Rev.* **2009**, *13*, 1372−1382.
(5) Saidur, R.; Islam, M.; Rahim, N.; Solangi, K. A Review on Global Wind Energy Policy. *Renewable Sustainable Energy Rev.* **2010**, *14*, 1744−1762.
(6) Bilgili, M.; Yasar, A.; Simsek, E. Offshore Wind Power Development in Europe and Its Comparison with Onshore Counterpart. *Renewable Sustainable Energy Rev.* **2011**, *15*, 905−915.
(7) Delucchi, M. A.; Jacobson, M. Z. Providing All Global Energy with Wind, Water, and Solar Power, Part II: Reliability, System and Transmission Costs, and Policies. *Energy Policy* **2011**, *39*, 1170−1190.
(8) Chen, Z.; Guerrero, J. M.; Blaabjerg, F. A Review of the State of the Art of Power Electronics for Wind Turbines. *IEEE Trans. Power Electr.* **2009**, *24*, 1859−1875.
(9) Bang, D.; Polinder, H.; Shrestha, G.; Ferreira, J. A. In Review of Generator Systems for Direct-Drive Wind Turbines, Presented at the European Wind Energy Conference & Exhibition, Belgium, 2008; pp 1−11.
(10) Pena, R.; Clare, J.; Asher, G. Doubly Fed Induction Generator Using Back-to-Back PWM Converters and Its Application to Variable-Speed Wind-Energy Generation. *IEEE Proc. Electr. Power Appl.* **1996**, *143*, 231−241.
(11) Chinchilla, M.; Arnaltes, S.; Burgos, J. C. Control of Permanent-Magnet Generators Applied to Variable-Speed Wind-Energy Systems Connected to the Grid. *IEEE Trans. Energy Convers.* **2006**, *21*, 130−135.
(12) Fan, F.-R.; Tian, Z.-Q.; Lin Wang, Z. Flexible Triboelectric Generator. *Nano Energy* **2012**, *1*, 328−334.
(13) Wang, Z. L. Triboelectric Nanogenerators as New Energy Technology for Self-Powered Systems and as Active Mechanical and Chemical Sensors. *ACS Nano* **2013**, *7*, 9533−9557.
(14) Zhu, G.; Pan, C.; Guo, W.; Chen, C. Y.; Zhou, Y.; Yu, R.; Wang, Z. L. Triboelectric-Generator-Driven Pulse Electrodeposition for Micropatterning. *Nano Lett.* **2012**, *12*, 4960−5.

(15) Zhu, G.; Chen, J.; Liu, Y.; Bai, P.; Zhou, Y. S.; Jing, Q.; Pan, C.; Wang, Z. L. Linear-Grating Triboelectric Generator Based on Sliding Electrification. *Nano Lett.* **2013**, *13*, 2282−9.
(16) Yang, Y.; Zhou, Y. S.; Zhang, H.; Liu, Y.; Lee, S.; Wang, Z. L. A Single-Electrode Based Triboelectric Nanogenerator as Self-Powered Tracking System. *Adv. Mater.* **2013**, *25*, 6594−601.
(17) Xie, Y.; Wang, S.; Lin, L.; Jing, Q.; Lin, Z.-H.; Niu, S.; Wu, Z.; Wang, Z. L. Rotary Triboelectric Nanogenerator Based on a Hybridized Mechanism for Harvesting Wind Energy. *ACS Nano* **2013**, *7*, 7119−7125.
(18) Yang, Y.; Zhu, G.; Zhang, H.; Chen, J.; Zhong, X.; Lin, Z.-H.; Su, Y.; Bai, P.; Wen, X.; Wang, Z. L. Triboelectric Nanogenerator for Harvesting Wind Energy and as Self-Powered Wind Vector Sensor System. *ACS Nano* **2013**, *7*, 9461−9468.
(19) Lin, Z. H.; Cheng, G.; Lin, L.; Lee, S.; Wang, Z. L. Water-Solid Surface Contact Electrification and Its Use for Harvesting Liquid-Wave Energy. *Angew. Chem.* **2013**, *52*, 12545−9.
(20) Zhu, G.; Bai, P.; Chen, J.; Lin Wang, Z. Power-Generating Shoe Insole Based on Triboelectric Nanogenerators for Self-Powered Consumer Electronics. *Nano Energy* **2013**, *2*, 688−692.
(21) Wang, S.; Lin, Z.-H.; Niu, S.; Lin, L.; Xie, Y.; Pradel, K. C.; Wang, Z. L. Motion Charged Battery as Sustainable Flexible-Power-Unit. *ACS Nano* **2013**, *7*, 11263−11271.
(22) Wang, S.; Lin, L.; Wang, Z. L. Nanoscale Triboelectric-Effect-Enabled Energy Conversion for Sustainably Powering Portable Electronics. *Nano Lett.* **2012**, *12*, 6339−6346.
(23) Zhou, Y. S.; Liu, Y.; Zhu, G.; Lin, Z.-H.; Pan, C.; Jing, Q.; Wang, Z. L. In Situ Quantitative Study of Nanoscale Triboelectrification and Patterning. *Nano Lett.* **2013**, *13*, 2771−2776.
(24) Niu, S.; Liu, Y.; Wang, S.; Lin, L.; Zhou, Y. S.; Hu, Y.; Wang, Z. L. Theoretical Investigation and Structural Optimization of Single-Electrode Triboelectric Nanogenerators. *Adv. Funct. Mater.* **2014**, DOI: 10.1002/adfm.201303799.
(25) Munson, B. R.; Young, D. F.; Okiishi, T. H. *Fundamentals of Fluid Mechanics*; Wiley: New York, 1990.
(26) Allen, J.; Smits, A. Energy Harvesting Eel. *J. Fluid. Struct.* **2001**, *15*, 629−640.
(27) Akaydin, H. D.; Elvin, N.; Andreopoulos, Y. Energy Harvesting from Highly Unsteady Fluid Flows Using Piezoelectric Materials. *J. Intell. Mater. Syst. Struct.* **2010**, *21*, 1263−1278.
(28) Robbins, W. P.; Morris, D.; Marusic, I.; Novak, T. O. Wind-Generated Electrical Energy Using Flexible Piezoelectric Mateials. *Proceedings of the ASME 2006 International Mechanical Engineering Congress and Exposition*; Chicago, Nov 5−10, 2006 ; ASME: New York, 2006; pp 581−590.
(29) Taylor, G. W.; Burns, J. R.; Kammann, S.; Powers, W. B.; Welsh, T. R. The Energy Harvesting Eel: A Small Subsurface Ocean/River Power Generator. *IEEE J. Oceanic Eng.* **2001**, *26*, 539−547.
(30) Akaydin, H.; Elvin, N.; Andreopoulos, Y. Wake of a Cylinder: A Paradigm for Energy Harvesting with Piezoelectric Materials. *Exp. Fluids* **2010**, *49*, 291−304.